ACS NANO

www.acsnano.org

ARTICLE

Sub-5 nm Contacts and Induced p−n Junction Formation in Individual Atomically Precise Graphene Nanoribbons

Pin-Chiao Huang, Hongye Sun, Mamun Sarker, Christopher M. Caroff, Gregory S. Girolami, Alexander Sinitskii, and Joseph W. Lyding*

Cite This: *ACS Nano* 2023, 17, 17771−17778

Read Online

ACCESS | Metrics & More | Article Recommendations | Supporting Information

ABSTRACT: **This paper demonstrates the fabrication of nanometer-scale metal contacts on individual graphene nanoribbons (GNRs) and the use of these contacts to control the electronic character of the GNRs. We demonstrate the use of a low-voltage direct-write STM-based process to pattern sub-5 nm metallic hafnium diboride (HfB_2) contacts directly on top of single GNRs in an ultrahigh-vacuum scanning tunneling microscope (UHV-STM), with all the fabrication performed on a technologically relevant semiconductor silicon substrate. Scanning tunneling spectroscopy (STS) data not only verify the expected metallic and semiconducting character of the contacts and GNR, respectively, but also show induced band bending and p−n junction formation in the GNR due to the metal−GNR work function difference. Contact engineering with different work function metals obviates the need to create GNRs with different characteristics by complex chemical doping. This is a demonstration of the successful fabrication of precise metal contacts and local p−n junction formation on single GNRs.**

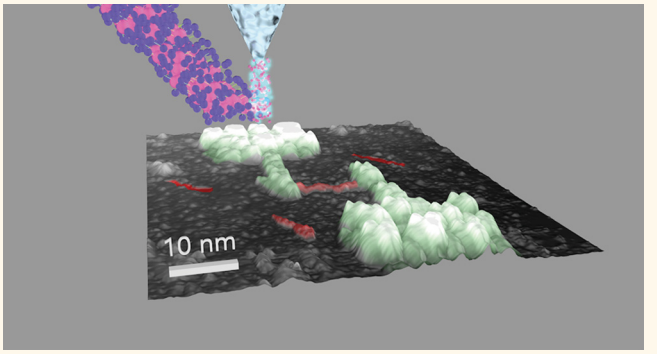

KEYWORDS: *graphene nanoribbon, scanning tunneling microscopy, scanning tunneling spectroscopy, electron-beam-induced deposition, hafnium diboride nanowires, silicon, nanostructures*

INTRODUCTION

Graphene nanoribbons (GNRs) are attracting great attention due to their electronic, optical, mechanical, and magnetic properties such as high electron mobility, broad-band light absorption, and high flexibility.[1−5] One useful property of GNRs is that their direct bandgaps can be tuned from 0 to over 3 eV depending on their structural parameters, such as ribbon width and edge structure, as well as a variety of external factors such as strain and doping.[6−10] Because of their small size, GNR field-effect transistors (GNRFETs) are of particular interest for the aggressive device scaling of microelectronic devices. To obtain suitable bandgaps and ensure acceptable GNRFET performance, however, a GNR lateral width of 1−2 nm is required[11], and the edge structure must be precisely controlled.[12] Top-down approaches to fabricate GNRs by e-beam lithography followed by etching and metal evaporation afford GNRs whose edges are not atomically precise.[13,14] Fortunately, atomically precise GNRs with smooth edges and narrow ribbon widths are now available in bulk quantities owing to recent developments in bottom-up synthesis.[10,15−20]

An important challenge is to discover ways to make metal contacts reproducibly with atomically precise GNRs. There have also been multiple attempts to fabricate electronic devices based on bottom-up synthesized GNRs prepared by on-surface[21−24] and solution methods[15−17,25,26] as well as chemical vapor deposition (CVD).[27,28] Regardless of the GNR type and the preparation method, a targeted fabrication of an electronic device around a preselected individual nanoribbon has not been demonstrated yet. The common fabrication challenges include the very small size of individual bottom-up synthesized GNRs (with typical widths of a couple of nm and typical lengths of a few tens of nm) as well as their tendency to aggregate in two-dimensional or three-dimensional

Received: March 27, 2023
Accepted: August 7, 2023
Published: August 15, 2023

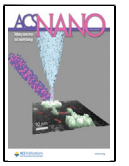

Scheme 1. Fabrication of Metallic Contacts on Individual GNRs: (a) DCT Deposition of GNRs on H:Si(100) Substrate,[a] (b) EBID of HfB_2 Metallic Contacts on a Selected GNR,[b] and (c) HfB_2 Metallic Contacts Drawn over an Individual GNR by the STM Tip

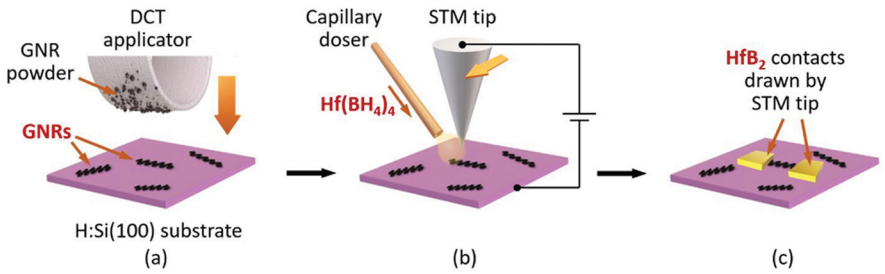

[a]A GNR powder is placed on a DCT applicator that is pressed against the substrate, resulting in exfoliation of some individual nanoribbons on H:Si(100). Individual GNRs for the contact fabrication can be located on a H:Si(100) substrate by STM. [b]HfB_2 is formed via local decomposition of $Hf(BH_4)_4$ that is guided by the STM tip. The STM tip is moved across the GNR to define the HfB_2 contacts.

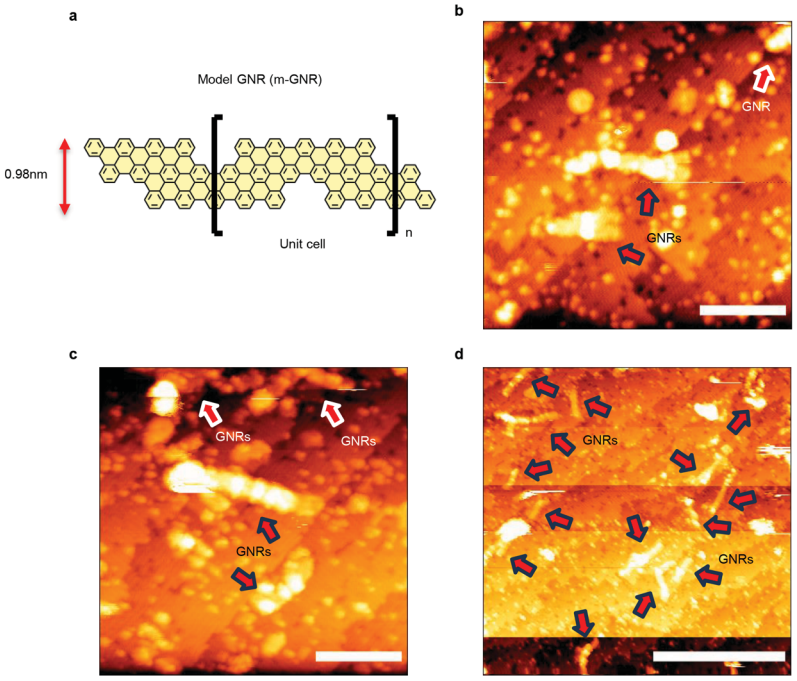

Figure 1. STM images of m-GNRs on H:Si(100): sample bias −2 V, tunneling current 10 pA. The locations of GNRs are indicated with red arrows. (a) Chemical structure of the m-GNR that was used in this study, showing a lateral width of 0.98 nm. (b) Image of an m-GNR chosen for making HfB_2 metallic contacts. Scale bar: 10 nm. (c) Image of another m-GNR. Scale bar: 10 nm. (d) Zoomed-out image showing numerous m-GNRs on the sample. Scale bar: 40 nm.

assemblies.[29,30] As a result, all prior attempts to electrically probe bottom-up synthesized GNRs focused on their various assemblies rather than individual ribbons. Typical fabrication procedures involve the lithographic fabrication of arrays of source (S) and drain (D) electrodes with an expectation that some of the deposited GNRs would bridge the gaps,[21] but such approaches lack control, precision, and efficiency. Besides, the GNRs connecting the S/D contacts are often clumped together, whether in series or in parallel, which hinders device performance considerably. Earlier approaches to fabricate electronic devices on larger top-down GNRs, that could be prepared lithographically,[13,14] sonochemically,[31] or by unzipping of carbon nanotubes,[32−34] also have their limitations. In these approaches, a GNR is typically located on the surface by microscopy, and then traditional lithographic methods (involving multiple deposition, irradiation, etch, and lift-off steps)[31] are used to form the metal contacts. But because GNRs are so small and fragile, it is extremely difficult to perform all these steps while maintaining precision on the nanoscale and without damaging the GNRs or introducing contamination that stochastically alters their properties.

A possible way to form contacts with GNRs that does not involve photo- or e-beam lithography is electron-beam-induced deposition (EBID),[35] but the high voltages of several kV typically used in this process will certainly damage the delicate GNRs. In 2010, we demonstrated the direct patterning of sub-5 nm HfB_2 metallic nanostructures at much smaller applied voltages of 5−7 eV:[36] the nanostructures were deposited from the carbon-free precursor $Hf(BH_4)_4$ onto H-passivated Si(100)-2 × 1 under UHV conditions by a process we call STM direct-write.

In this study, we show that STM direct-write nanometalization can enable the deposition of metal electrodes onto the opposite ends of a single GNR, which is an important

https://doi.org/10.1021/acsnano.3c02794
ACS Nano 2023, 17, 17771−17778

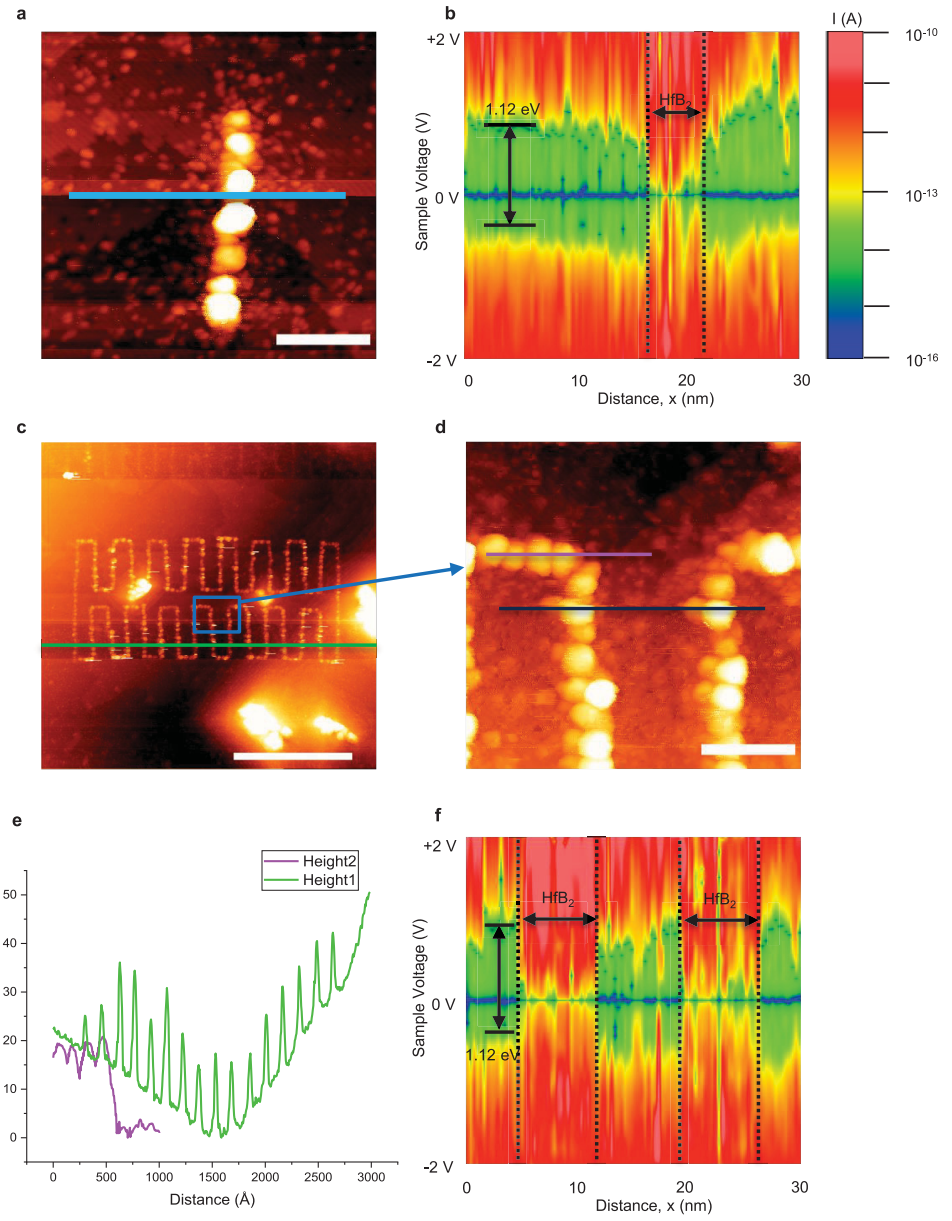

Figure 2. HfB_2 metal nanostructures. (a) A sub-5 nm wide line of HfB_2 deposited on H:Si(100). H-passivated Si dimer rows are shown in the background. Dangling bonds are noted. The average height of the line is about 2.3 nm. Deposition conditions: sample bias = 7 V, I = 0.1 nA, writing dose = 10^{-4} C/cm, writing time = 15 s (10 nm/s). The writing repeat count was 5, with each attempt taking 3 s. $Hf(BH_4)_4$ background pressure: 1.6×10^{-9} Torr. The scale bar is 10 nm. (b) A 30 nm long STS map (along light blue line in (a)) showing metallic behavior at the HfB_2 line and semiconducting behavior on the substrate (H:Si(100)). Band-bending is observed between Si and HfB_2. (c) Serpentine nanostructure of HfB_2. The scale bar is 100 nm. (d) Zoomed-in image of the blue box area in (c), showing HfB_2 structural continuity. The scale bar is 10 nm. (e) Height vs distance analysis (green line in (c) and purple line in (d), respectively) of the HfB_2 nanostructure showing vertical features due to the HfB_2 deposits, which are about 1−2 nm tall. The roughness of HfB_2 is within 1 nm. (f) STS map (along the black line in (d)) showing a bandgap of 0 eV at the HfB_2 line and 1.1 eV on the substrate. For the STM images in (a) and (c), the sample bias was −2 V and the tunneling current was 10 pA.

step toward creating single GNR transistors. We demonstrate the successful fabrication of precise metal contacts with single GNRs. This approach, importantly, facilitates the use of the metal−GNR work function difference to engineer band bending in the GNR, thus achieving n- or p-type doping, Ohmic contacts, p−n junction formation, or more complex heterostructures. Such work function control is used in current silicon technology to avoid the stochastic fluctuations in dopants that would otherwise have to be used in the silicon channel region. This work function effect and p−n junction formation are demonstrated in this paper. Importantly, the described patterning approach is applicable to GNRs on a multitude of different surfaces and is demonstrated here for nanoribbons deposited on a technologically relevant semiconductor silicon substrate.

RESULTS AND DISCUSSION

The general procedure for the fabrication of HfB_2 metallic contacts on an individual atomically precise GNR is shown in Scheme 1. In brief, the GNRs are first deposited on a H:Si(100) using a dry contact transfer (DCT) method

https://doi.org/10.1021/acsnano.3c02794
ACS Nano 2023, 17, 17771−17778

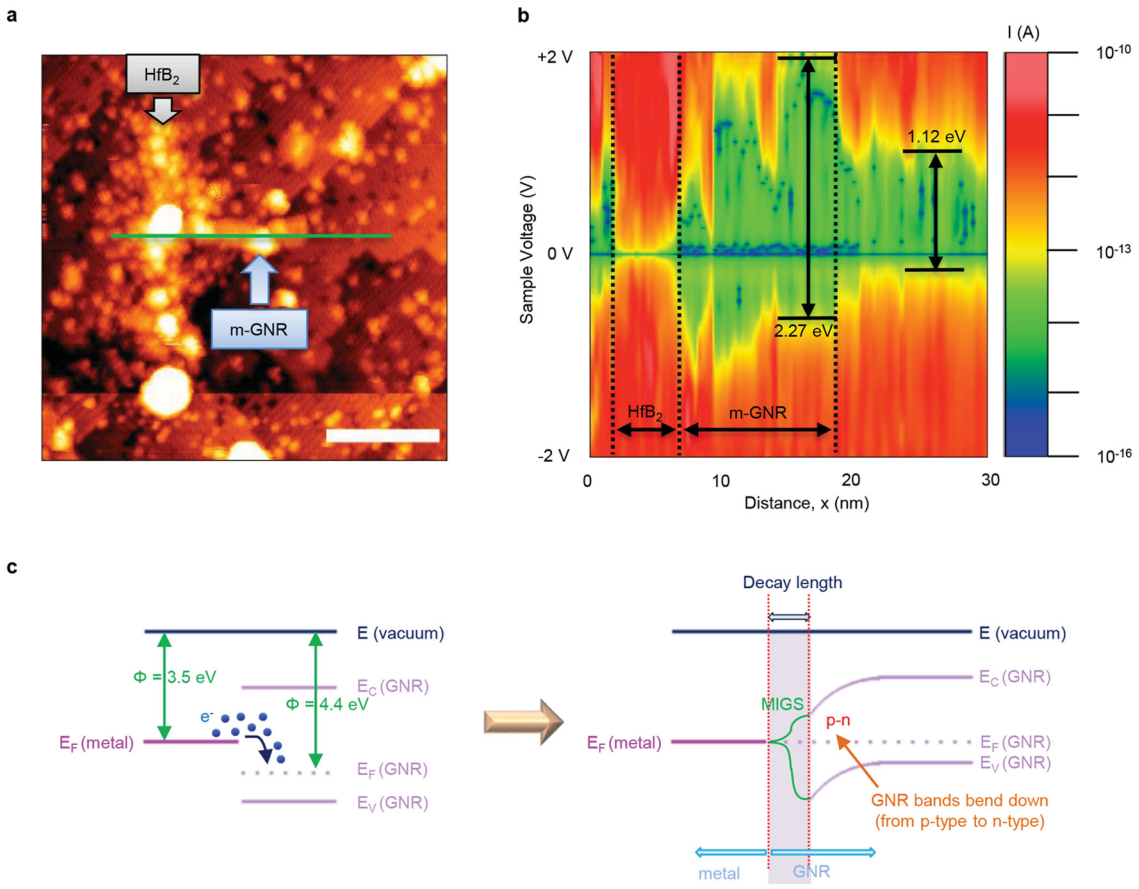

Figure 3. STM direct writing of HfB_2 nanowires across an m-GNR. (a) STM image after direct nanometalization writing of the HfB_2 line across the left side of an m-GNR on H:Si(100). The average thickness of the line is about 1.5 nm. Deposition conditions: sample bias 7 V, I = 0.1 nA, writing dose 10^{-4} C/cm, and writing time 2.6 s (10 nm/s). $Hf(BH_4)_4$ background pressure: 3.6 × 10^{-9} Torr. The scale bar is 10 nm. (b) STS results (green line in (a)) showing a strong band-bending effect on m-GNR due to the low work function of HfB_2 (3.5 eV). Metallic behavior at HfB_2, the semiconductor nature of the m-GNR, and substrate bandgap (1.12 eV) are shown. (c) Band diagram explaining induced band-bending in m-GNR.

(Scheme 1a) developed by our group; this method has previously been used to transfer carbon nanotubes (CNTs),[37] exfoliated graphene,[12,38] and GNRs[16,17,39] onto surfaces under UHV conditions. In this method, a powder of solution-synthesized GNRs is first annealed under UHV conditions to remove residual solvent molecules and other adsorbates and then, while still in a UHV chamber, pressed against a clean substrate, which results in exfoliation of some ribbons to the surface. We previously used the DCT approach to deliver several kinds of structurally related solution-synthesized GNRs to semiconductor substrates, such as H:Si(100) and InAs (110), and demonstrated adsorbate-free samples that were suitable for STS characterization.[16,17,39] Because the process is performed directly in the UHV chamber of an STM instrument, the exfoliated GNRs can be visualized by STM and some of them can be selected for contact patterning. The patterning is then performed using the STM-EBID process that is illustrated by Scheme 1b. This process employs a capillary doser that delivers $Hf(BH_4)_4$ directly to the H:Si(100) surface with GNRs. When a potential difference is applied between the STM tip and the substrate, this promotes the local decomposition of $Hf(BH_4)_4$ into metallic HfB_2 that forms directly under the tip. By moving the STM tip across the GNR, it is therefore possible to directly draw HfB_2 contacts on a single nanoribbon, as illustrated by Scheme 1c.

For this study, we used solution-synthesized GNRs with a structure shown in Figure 1a. Since this GNR served as a model graphene nanoribbon (m-GNR) for the STM-EBID process, we do not provide here its detailed synthetic procedure or characterization, which will be published separately. Suffice it to say that for the purpose of exfoliation onto H:Si(100) by DCT, which is the important first step of the described procedure (Scheme 1), these ribbons behaved similarly to the previously studied chevron GNRs[39] and laterally extended chevron GNRs,[16,17] which could have served as model nanoribbons as well. As a result, the focus of this article rests on the contacts and interactions between HfB_2 and a single m-GNR.

Figure 1b,c shows the STM topographic images of freshly deposited m-GNRs (i.e., before any metal contacts are created). The quantity of m-GNRs on the H:Si(100) sample surface seen in Figure 1d enables us to conduct direct metalization easily on multiple m-GNR candidates. This demonstrates that the DCT was successful and that there are multiple m-GNRs from which to choose.

Before forming metallic nanocontacts with the m-GNRs, we first reproduced our ability to deposit HfB_2 lines by the STM direct-write method.[36] HfB_2 is a metallic ceramic with a room-temperature bulk resistivity of only 7 $\mu\Omega$ cm[40] that is lower than the resistivity of platinum. The HfB_2 precursor molecule

https://doi.org/10.1021/acsnano.3c02794
ACS Nano 2023, 17, 17771−17778

$Hf(BH_4)_4$ was introduced into an STM chamber through a 1 mm diameter stainless steel capillary whose orifice was positioned close to the STM probe tip. The capillary creates a relatively high local precursor pressure near the tip while the chamber is maintained at near-background pressures. To effect HfB_2 deposition, the STM probe was operated at a bias of 7 V (probe negative) and a current of 0.1 nA; the total electron dose was 10^{-4} C/cm. When gaseous molecules of $Hf(BH_4)_4$ diffuse into the STM electron beam, they fragment to give HfB_2, which forms a deposit on the surface; if the STM tip is moved across the surface, it leaves a line of HfB_2 behind. This process also produces hydrogen and diborane, which are volatile and leave the reaction zone.

To assess the quality of the HfB_2 metal lines before using them to make nanocontacts with the m-GNRs, we wrote various patterns such as square plates, grids of lines, and serpentine nanostructures onto regions of the H:Si(100) surface that were free of GNRs (Figure 2). The HfB_2 deposition was conducted at a writing speed of 10 nm/s, and to compensate for potential HfB_2 nucleation delays, the writing process was repeated 5 times. A thicker and more uniform HfB_2 deposit can be achieved simply by scanning the STM probe over a line more times.

We see an increase in dangling bond density in the vicinity of written HfB_2 features, presumably when the atomic hydrogen released from the precursor molecules during the writing process reacts with surface hydrogen to produce H_2 plus dangling bonds, as we have seen in our previous work.[36] There are also large bright features that we assume to be SiC contamination that arise from incomplete carbon removal during high-temperature surface cleaning (Figure 2c). The sample preparation temperature in Figure 2c did not go above 960 °C, and SiC on Si results in a pyramidlike shape, as seen in our data. Scanning tunneling spectroscopy (STS) studies show the typical 1.12 eV band gap for the H:Si(100) surface but no band gap for the STM direct-write features; the latter finding is consistent with the deposition of metallic HfB_2 (Figure 2b,f). A band-bending effect of Si in the vicinity of HfB_2 is also prominent in Figure 2b due to the work function difference, creating a Schottky barrier. An expanded view of a small area of the serpentine nanostructure (Figure 2d) suggests that the HfB_2 deposits are continuous despite their beadlike appearance: height analysis reveals the surface roughness along the HfB_2 line to be <1 nm (purple line in Figure 2d, result in Figure 2e). The height vs distance analysis taken along the green line in Figure 2c shows a regular pattern of equally spaced HfB_2 lines having heights of about 1−2 nm, written onto an underlying Si surface that is not flat but instead exhibits a trough in the center of the scan that is about 3 nm deep (Figure 2e). The result shows that the STM direct writing process is robust and adaptable enough to deposit continuous lines even onto surfaces that exhibit significant variations in surface height.

The STM direct-write method was then used to deposit a HfB_2 metal contact on the left end of an m-GNR; the writing speed was 10 nm/s, and the entire HfB_2 deposition process took approximately 2 s. An STM image shows that the HfB_2 line is around 26 nm long and 4 nm wide (Figure 3a). The large amount of deposition seen at one end of the metal line is possibly a consequence of something loose that came off the tip at the start of the write process.

Figure 3b shows that the unpatterned portion of a m-GNR is semiconducting and has a bandgap larger than 2 eV, which is consistent with our prior measurements of other structurally related chevron-family GNRs on H:Si(100) and InAs(110) substrates.[16,17,39] A detailed spectroscopic and theoretical study of individual m-GNRs on H:Si(100) will be published separately, while here we are focusing on their nanometalization and electronic properties of their interfaces with HfB_2 contacts. STS studies of HfB_2 nanometalized m-GNRs show that there is a strong band-bending effect, to the extent that the m-GNR shows n-type instead of p-type behavior (Figure 3b). This induced band-bending effect is likely due to the low work function of HfB_2 (3.5 eV),[41] which will cause electrons to flow across the junction to the m-GNRs. More data on m-GNR band bending can be found in Figure S3. The band-bending suggests that the interface between HfB_2 and m-GNRs is most likely an Ohmic contact, with the GNR becoming degenerate n-type beneath the HfB_2. The band-bending effect creates a local p−n junction in the m-GNR. To date, the general consensus in nanotechnology is that to advance GNR electronics we need to make all kinds of different GNRs (n-type, p-type, metallic, etc.) and then combine them into complex heterostructures. This is extremely difficult to do, and the success has been very limited so far. Therefore, our approach is to use contact-induced doping to replace the need for incorporation of dopant atoms into GNRs. As a consequence, essentially any semiconducting GNR can be used for device fabrication. Notably, today's silicon technology uses the gate metal work function to tune the band-bending of the silicon channel and achieve doping without the use of dopants.[42−44]

Even though the topographic image (Figure 3a) shows a sharp junction boundary between HfB_2 and m-GNR, the transition from semiconducting to metallic behavior across the junction (as revealed by the bandgap changes) is not abrupt. Instead, there is a transition region within the GNR across which the bandgap increases gradually from that characteristic of HfB_2 to that seen for isolated m-GNRs. The lower bandgap (and resulting enhanced conductivity) in the transition region is attributed to the presence of metal-induced gap states (MIGS) in the m-GNR, the decay length of which is about 2.4 nm as judged from the STS map. Similar transition regions have been reported by Ruppalt et al. for metal−semiconductor CNT heterojunctions.[45]

The work function of isolated m-GNRs has not previously been measured or calculated, but for unstrained armchair GNRs it was previously theoretically predicted to be 4.3 eV.[46] It can be seen in Figure 3b that the intrinsic m-GNR Fermi level is slightly offset toward the valence band edge with $E_F - E_v \approx 0.5$ eV at the Si interface; this offset is due to charge transfer with the p-type H:Si(100) surface, which has a work function of 4.91 eV[17,39] (electrons flow out of the m-GNR into the higher work function Si). This result indicates that the work function of the m-GNRs is approximately equal to 4.9 − 0.5 = 4.4 eV, which agrees with the theoretical estimate. Furthermore, the zero-order expected band-bending should be the work function difference of the m-GNRs and HfB_2 (4.4 − 3.5 = 0.9 eV). We observe about 0.6 eV band bending, which is reasonable given the possible effects of stoichiometric variations in the hafnium diboride work function and the effect of substrate−GNR interactions. We will explore these effects in greater detail in future work.

To explore the possibility of creating GNR-based transistors, we used the STM direct-write nanometalization method at a writing speed of 5 nm/s to fabricate HfB_2 metal contacts

https://doi.org/10.1021/acsnano.3c02794
ACS Nano 2023, 17, 17771−17778

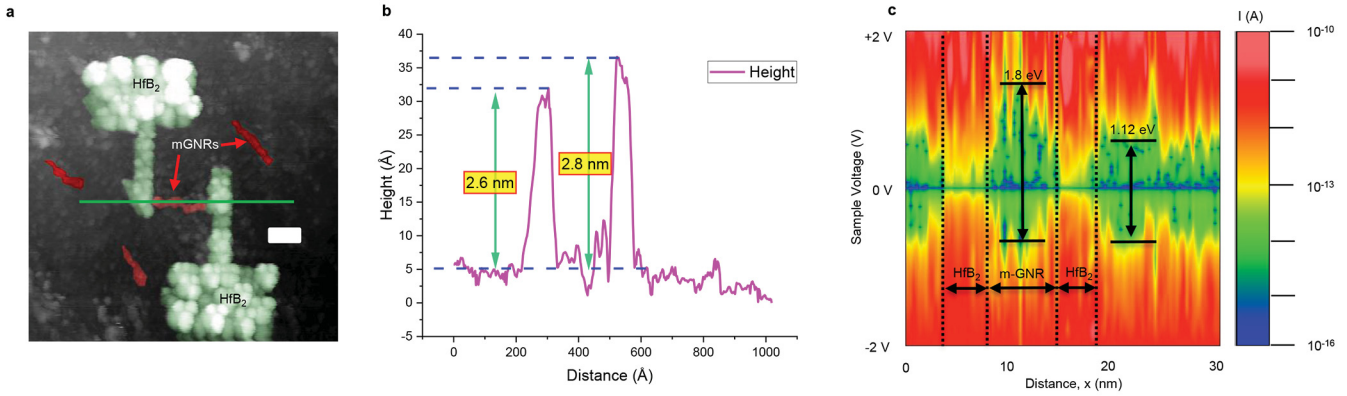

Figure 4. M-GNR metal contact pads. (a) STM-EBID direct nanometalization of HfB_2 on a m-GNR to form contact pads for future transport measurements. Deposition conditions: sample bias 7 V, current 0.1 nA, and writing dose = 10^{-4} C/cm. $Hf(BH_4)_4$ background pressure: 5.8 × 10^{-9} Torr. HfB_2 and m-GNRs are colored green and red, respectively. The scale bar is 10 nm. (b) Height analysis along the green line in (a). (c) STM spectroscopy (STS) acquired along the green line in (a), showing Si, metallic HfB_2, and larger bandgap of the m-GNR.

(which could be used as source and drain terminals) on both ends of a single m-GNR (Figure 4a). Figure 1a shows a schematic illustration of the m-GNR chemical structure with a lateral width of 1.0 nm, excluding the distance of hydrogen atoms and their van der Waals surfaces that terminate the armchair edges, whereas the width of the HfB_2 line is under 4 nm. Both contact pad features are approximately 2.7 nm in height (Figure 4b). The STS data correspond well to the expected bandgaps of all regions (Figure 4c): metallic behavior for HfB_2 and semiconducting behavior for Si and m-GNR.

CONCLUSIONS

We have demonstrated precise control over the fabrication of single-GNR metal contacts using STM direct nanometalization as the fabrication method and HfB_2 as the metallic conductor. Owing to the small work function of HfB_2, there is band-bending near the junction, which can be beneficial in some applications because a local p−n junction is created at the contact. By changing the metal precursors we use, however, we can deposit other metals with different work functions, if desired. Because armchair-shaped GNRs have direct bandgaps due to quantum confinement and the presence of Dirac cones,[2,6,47] devices containing single GNR p−n junctions would be attractive materials for a variety of applications, especially in electronic and photonic devices.

The results herein show that STM direct-write nanometalization is a simple, clean, and fast way to deposit metallic contacts onto GNRs. Future transport measurements on single GNR transistors are needed to verify the integrity of the contacts, but the results to date hold promise that the STM direct-write approach could enable the construction of GNRFETs, logic gates, and photovoltaic devices.

METHODS

Synthesis of $Hf(BH_4)_4$. $Hf(BH_4)_4$ was synthesized according to a literature procedure.[48] $Hf(BH_4)_4$ is a solid that has a vapor pressure of 15 Torr at 25 °C.[49]

m-GNR Synthesis. m-GNR was synthesized in solution from DBDT (6,11-dibromo-1,4-diphenyltriphenylene) and DBTP (2,2′-[1,1′:4′,1″-terphenyl]-2′,5′-diylbis[4,4,5,5-tetramethyl-1,3,2-dioxaborolane]) via a Suzuki-polymerization reaction followed by a $FeCl_3$-mediated cyclodehydrogenation reaction. The detailed synthetic procedure and characterization of this GNR will be published separately.

Si Substrate Preparation and STM Experiments. An 8.5 × 4 mm silicon sample was cut with a diamond scriber from a B-doped p-type Si wafer (resistivity 0.01−0.02 Ω cm). The sample was sonicated in an acetone bath for 15 min and, subsequently, in an isopropyl alcohol bath for another 15 min. H passivation of the Si sample was carried out at 377 °C for 10 min and an H_2 background pressure of 2 × 10^{-6} Torr. Prior to H passivation, residual oxide was removed from the Si(100) substrates by heating them at 850 °C for 12 h and subsequently to 1205 °C several times as needed for 30 s.

All the experiments were conducted in a UHV home-built STM chamber[50] with a base pressure of less than 8 × 10^{-11} Torr. STM imaging was performed under constant current mode (sample bias −2 V; tunneling current 10^{-11} A) with iridium-coated tungsten probes manufactured by Tiptek, LLC. STS data were collected at predefined positions by recording the tunneling current change with a voltage sweep of −2 to +2 V, while moving the probe closer to the surface by 0.2 nm in a v-shaped ramp between the endpoint voltages and 0 V.

HfB_2 Deposition. The gas system consists of a glass vial that holds the $Hf(BH_4)_4$ precursor, a leak valve that controls the flow of the precursor into the STM chamber, and a 0.4 mm inner diameter stainless steel capillary doser whose orifice is positioned about 1 cm from the tip−sample junction. The electron energy provided by the STM probe is sufficient to dissociate $Hf(BH_4)_4$ into HfB_2, B_2H_6, and H. The last two byproducts are gases that are removed from the STM chamber with an ion pump.

ASSOCIATED CONTENT

Supporting Information

The Supporting Information is available free of charge at https://pubs.acs.org/doi/10.1021/acsnano.3c02794.

Original grayscale images for Figures 1 and 4a and additional data on a HfB_2 contacted m-GNR band-bending (PDF)

AUTHOR INFORMATION

Corresponding Author

Joseph W. Lyding − *Holonyak Micro and Nanotechnology Laboratory and Department of Electrical and Computer Engineering, University of Illinois at Urbana—Champaign, Urbana, Illinois 61801, United States;* orcid.org/0000-0001-7285-4310; Email: lyding@illinois.edu

Authors

Pin-Chiao Huang − *Holonyak Micro and Nanotechnology Laboratory and Department of Electrical and Computer Engineering, University of Illinois at Urbana—Champaign,*

https://doi.org/10.1021/acsnano.3c02794
ACS Nano 2023, 17, 17771−17778

Urbana, Illinois 61801, United States; orcid.org/0000-0002-1002-4183

Hongye Sun − *Holonyak Micro and Nanotechnology Laboratory and Department of Materials Science and Engineering, University of Illinois at Urbana—Champaign, Urbana, Illinois 61801, United States;* orcid.org/0000-0001-9135-8048

Mamun Sarker − *Department of Chemistry, University of Nebraska—Lincoln, Lincoln, Nebraska 68588, United States;* Present Address: Department of Applied Chemistry and Chemical Engineering, Noakhali Science and Technology University, Noakhali, Bangladesh; orcid.org/0000-0002-1541-7066

Christopher M. Caroff − *School of Chemical Sciences, University of Illinois at Urbana—Champaign, Urbana, Illinois 61801, United States*

Gregory S. Girolami − *School of Chemical Sciences, University of Illinois at Urbana—Champaign, Urbana, Illinois 61801, United States*

Alexander Sinitskii − *Department of Chemistry and Nebraska Center for Materials and Nanoscience, University of Nebraska—Lincoln, Lincoln, Nebraska 68588, United States;* orcid.org/0000-0002-8688-3451

Complete contact information is available at: https://pubs.acs.org/10.1021/acsnano.3c02794

Author Contributions

P.-C.H. and H.S. contributed equally to this paper. M.S. and A.S. synthesized the GNRs. C.M.C and G.S.G. synthesized $Hf(BH_4)_4$. P.-C.H., H.S., and J.W.L. conducted the STM experiments. The results were discussed among all authors, and all authors have given approval to the final version of the manuscript.

Funding

The research on the synthesis of GNRs was supported by the Office of Naval Research (ONR) through grant number N00014-19-1-2596. The STM experiments by P.-C.H., H.S., and J.W.L. were supported by the Office of Naval Research (ONR) through grant number N00014-19-1-2596 and by the Army Research Office (ARO) through grant number W911NF-18-1-0117. The synthetic work on $Hf(BH_4)_4$ by C.M.C. and G.S.G. was supported by the National Science Foundation under grant number CHE 19-54745.

Notes

The authors declare no competing financial interest.

ABBREVIATIONS

GNR, graphene nanoribbon; EBID, electron-beam-induced deposition; STM, scanning tunneling microscopy; AFM, atomic force microscopy; UHV, ultrahigh vacuum; STS, scanning tunneling spectroscopy; DCT, dry contact transfer; FET, field-effect transistor; CVD, chemical vapor deposition; CNT, carbon nanotube; MIGS, metal-induced gap states

REFERENCES

(1) Betti, A.; Fiori, G.; Iannaccone, G.; Mao, Y. Physical Insights on Graphene Nanoribbon Mobility through Atomistic Simulations. *Technol. Dig. - Int. Electron Devices Meet. IEDM* **2009**, 897−900.

(2) Son, Y.-W.; Cohen, M. L.; Louie, S. G. Energy Gaps in Graphene Nanoribbons. *Phys. Rev. Lett.* **2006**, *97* (21), No. 216803.

(3) Sasaki, K.; Kato, K.; Tokura, Y.; Oguri, K.; Sogawa, T. Theory of Optical Transitions in Graphene Nanoribbons. *Phys. Rev. B* **2011**, *84* (8), No. 085458.

(4) Wei, N.; Xu, L.; Wang, H.-Q.; Zheng, J.-C. Strain Engineering of Thermal Conductivity in Graphene Sheets and Nanoribbons: A Demonstration of Magic Flexibility. *Nanotechnology* **2011**, *22* (10), No. 105705.

(5) Yazyev, O. V. A Guide to the Design of Electronic Properties of Graphene Nanoribbons. *Acc. Chem. Res.* **2013**, *46* (10), 2319−2328.

(6) Yang, L.; Park, C.-H.; Son, Y.-W.; Cohen, M. L.; Louie, S. G. Quasiparticle Energies and Band Gaps in Graphene Nanoribbons. *Phys. Rev. Lett.* **2007**, *99* (18), No. 186801.

(7) Peng, X.; Velasquez, S. Strain Modulated Band Gap of Edge Passivated Armchair Graphene Nanoribbons. *Appl. Phys. Lett.* **2011**, *98* (2), 23112.

(8) Kimouche, A.; Ervasti, M. M.; Drost, R.; Halonen, S.; Harju, A.; Joensuu, P. M.; Sainio, J.; Liljeroth, P. Ultra-Narrow Metallic Armchair Graphene Nanoribbons. *Nat. Commun.* **2015**, *6* (1), 10177.

(9) Ruffieux, P.; Cai, J.; Plumb, N. C.; Patthey, L.; Prezzi, D.; Ferretti, A.; Molinari, E.; Feng, X.; Müllen, K.; Pignedoli, C. A.; Fasel, R. Electronic Structure of Atomically Precise Graphene Nanoribbons. *ACS Nano* **2012**, *6* (8), 6930−6935.

(10) Vo, T. H.; Shekhirev, M.; Kunkel, D. A.; Orange, F.; Guinel, M. J.-F.; Enders, A.; Sinitskii, A. Bottom-up Solution Synthesis of Narrow Nitrogen-Doped Graphene Nanoribbons. *Chem. Commun.* **2014**, *50* (32), 4172−4174.

(11) Fiori, G.; Iannaccone, G. Simulation of Graphene Nanoribbon Field-Effect Transistors. *IEEE Electron Device Lett.* **2007**, *28* (8), 760−762.

(12) Ritter, K. A.; Lyding, J. W. The Influence of Edge Structure on the Electronic Properties of Graphene Quantum Dots and Nanoribbons. *Nat. Mater.* **2009**, *8* (3), 235−242.

(13) Chen, Z.; Lin, Y.-M.; Rooks, M. J.; Avouris, P. Graphene Nano-Ribbon Electronics. *Phys. E Low-dimensional Syst. Nanostructures* **2007**, *40* (2), 228−232.

(14) Han, M. Y.; Brant, J. C.; Kim, P. Electron Transport in Disordered Graphene Nanoribbons. *Phys. Rev. Lett.* **2010**, *104* (5), No. 056801.

(15) Kim, K. T.; Jung, J. W.; Jo, W. H. Synthesis of Graphene Nanoribbons with Various Widths and Its Application to Thin-Film Transistor. *Carbon N. Y.* **2013**, *63*, 202−209.

(16) Liu, X.; Li, G.; Lipatov, A.; Sun, T.; Mehdi Pour, M.; Aluru, N. R.; Lyding, J. W.; Sinitskii, A. Chevron-Type Graphene Nanoribbons with a Reduced Energy Band Gap: Solution Synthesis, Scanning Tunneling Microscopy and Electrical Characterization. *Nano Res.* **2020**, *13* (6), 1713−1722.

(17) Mehdi Pour, M.; Lashkov, A.; Radocea, A.; Liu, X.; Sun, T.; Lipatov, A.; Korlacki, R. A.; Shekhirev, M.; Aluru, N. R.; Lyding, J. W.; et al. Laterally Extended Atomically Precise Graphene Nanoribbons with Improved Electrical Conductivity for Efficient Gas Sensing. *Nat. Commun.* **2017**, *8* (1), 820.

(18) Narita, A.; Feng, X.; Hernandez, Y.; Jensen, S. A.; Bonn, M.; Yang, H.; Verzhbitskiy, I. A.; Casiraghi, C.; Hansen, M. R.; Koch, A. H. R.; et al. Synthesis of Structurally Well-Defined and Liquid-Phase-Processable Graphene Nanoribbons. *Nat. Chem.* **2014**, *6* (2), 126−132.

(19) Cai, J.; Ruffieux, P.; Jaafar, R.; Bieri, M.; Braun, T.; Blankenburg, S.; Muoth, M.; Seitsonen, A. P.; Saleh, M.; Feng, X.; et al. Atomically Precise Bottom-up Fabrication of Graphene Nanoribbons. *Nature* **2010**, *466* (7305), 470−473.

(20) Vo, T. H.; Shekhirev, M.; Kunkel, D. A.; Morton, M. D.; Berglund, E.; Kong, L.; Wilson, P. M.; Dowben, P. A.; Enders, A.; Sinitskii, A. Large-Scale Solution Synthesis of Narrow Graphene Nanoribbons. *Nat. Commun.* **2014**, *5* (1), 3189.

(21) Bennett, P. B.; Pedramrazi, Z.; Madani, A.; Chen, Y.-C.; deOteyza, D. G.; Chen, C.; Fischer, F. R.; Crommie, M. F.; Bokor, J. Bottom-up Graphene Nanoribbon Field-Effect Transistors. *Appl. Phys. Lett.* **2013**, *103* (25), No. 253114.

(22) Llinas, J. P.; Fairbrother, A.; Borin Barin, G.; Shi, W.; Lee, K.; Wu, S.; Yong Choi, B.; Braganza, R.; Lear, J.; Kau, N. Short-Channel Field-Effect Transistors with 9-Atom and 13-Atom Wide Graphene Nanoribbons. *Nat. Commun.* **2017**, *8* (1), 633.

(23) ElAbbassi, M.; Perrin, M. L.; Barin, G. B.; Sangtarash, S.; Overbeck, J.; Braun, O.; Lambert, C. J.; Sun, Q.; Prechtl, T.; Narita, A.; et al. Controlled Quantum Dot Formation in Atomically Engineered Graphene Nanoribbon Field-Effect Transistors. *ACS Nano* **2020**, *14* (5), 5754−5762.
(24) Borin Barin, G.; Sun, Q.; DiGiovannantonio, M.; Du, C.; Wang, X.; Llinas, J. P.; Mutlu, Z.; Lin, Y.; Wilhelm, J.; Overbeck, J. Growth Optimization and Device Integration of Narrow-Bandgap Graphene Nanoribbons. *Small* **2022**, *18* (31), No. 2202301.
(25) Shekhirev, M.; Vo, T. H.; Mehdi Pour, M.; Lipatov, A.; Munukutla, S.; Lyding, J. W.; Sinitskii, A. Interfacial Self-Assembly of Atomically Precise Graphene Nanoribbons into Uniform Thin Films for Electronics Applications. *ACS Appl. Mater. Interfaces* **2017**, *9* (1), 693−700.
(26) Niu, W.; Sopp, S.; Lodi, A.; Gee, A.; Kong, F.; Pei, T.; Gehring, P.; Nägele, J.; Lau, C. S.; Ma, J.; et al. Exceptionally Clean Single-Electron Transistors from Solutions of Molecular Graphene Nanoribbons. *Nat. Mater.* **2023**, *22* (2), 180−185.
(27) Chen, Z.; Zhang, W.; Palma, C.-A.; Lodi Rizzini, A.; Liu, B.; Abbas, A.; Richter, N.; Martini, L.; Wang, X.-Y.; Cavani, N. Synthesis of Graphene Nanoribbons by Ambient-Pressure Chemical Vapor Deposition and Device Integration. *J. Am. Chem. Soc.* **2016**, *138* (47), 15488−15496.
(28) Shekhirev, M.; Lipatov, A.; Torres, A.; Vorobeva, N. S.; Harkleroad, A.; Lashkov, A.; Sysoev, V.; Sinitskii, A. Highly Selective Gas Sensors Based on Graphene Nanoribbons Grown by Chemical Vapor Deposition. *ACS Appl. Mater. Interfaces* **2020**, *12* (6), 7392−7402.
(29) Shekhirev, M.; Vo, T. H.; Kunkel, D. A.; Lipatov, A.; Enders, A.; Sinitskii, A. Aggregation of Atomically Precise Graphene Nanoribbons. *Rsc Adv.* **2017**, *7* (86), 54491−54499.
(30) Vo, T. H.; Perera, U. G. E.; Shekhirev, M.; Mehdi Pour, M.; Kunkel, D. A.; Lu, H.; Gruverman, A.; Sutter, E.; Cotlet, M.; Nykypanchuk, D.; et al. Nitrogen-Doping Induced Self-Assembly of Graphene Nanoribbon-Based Two-Dimensional and Three-Dimensional Metamaterials. *Nano Lett.* **2015**, *15* (9), 5770−5777.
(31) Wang, X.; Ouyang, Y.; Li, X.; Wang, H.; Guo, J.; Dai, H. Room-Temperature All-Semiconducting Sub-10-Nm Graphene Nanoribbon Field-Effect Transistors. *Phys. Rev. Lett.* **2008**, *100* (20), No. 206803.
(32) Jiao, L.; Zhang, L.; Wang, X.; Diankov, G.; Dai, H. Narrow Graphene Nanoribbons from Carbon Nanotubes. *Nature* **2009**, *458* (7240), 877−880.
(33) Kosynkin, D. V.; Higginbotham, A. L.; Sinitskii, A.; Lomeda, J. R.; Dimiev, A.; Price, B. K.; Tour, J. M. Longitudinal Unzipping of Carbon Nanotubes to Form Graphene Nanoribbons. *Nature* **2009**, *458* (7240), 872−876.
(34) Sinitskii, A.; Fursina, A. A.; Kosynkin, D. V.; Higginbotham, A. L.; Natelson, D.; Tour, J. M. Electronic Transport in Monolayer Graphene Nanoribbons Produced by Chemical Unzipping of Carbon Nanotubes. *Appl. Phys. Lett.* **2009**, *95* (25), No. 253108.
(35) Greve, M. M.; Holst, B. Optimization of an Electron Beam Lithography Instrument for Fast, Large Area Writing at 10 KV Acceleration Voltage. *J. Vac. Sci. Technol. B, Nanotechnol. Microelectron. Mater. Process. Meas. Phenom.* **2013**, *31* (4), 43202.
(36) Ye, W.; Peña Martin, P. A.; Kumar, N.; Daly, S. R.; Rockett, A. A.; Abelson, J. R.; Girolami, G. S.; Lyding, J. W. Direct Writing of Sub-5 Nm Hafnium Diboride Metallic Nanostructures. *ACS Nano* **2010**, *4* (11), 6818−6824.
(37) Albrecht, P. M.; Lyding, J. W. Ultrahigh-Vacuum Scanning Tunneling Microscopy and Spectroscopy of Single-Walled Carbon Nanotubes on Hydrogen-Passivated Si(100) Surfaces. *Appl. Phys. Lett.* **2003**, *83* (24), 5029−5031.
(38) Ritter, K. A.; Lyding, J. W. Characterization of Nanometer-Sized, Mechanically Exfoliated Graphene on the H-Passivated Si (100) Surface Using Scanning Tunneling Microscopy. *Nanotechnology* **2008**, *19* (1), No. 015704.
(39) Radocea, A.; Sun, T.; Vo, T. H.; Sinitskii, A.; Aluru, N. R.; Lyding, J. W. Solution-Synthesized Chevron Graphene Nanoribbons Exfoliated onto H: Si(100). *Nano Lett.* **2017**, *17* (1), 170−178.
(40) Zhang, L.; Pejaković, D. A.; Marschall, J.; Gasch, M. Thermal and Electrical Transport Properties of Spark Plasma-sintered HfB2 and ZrB2 Ceramics. *J. Am. Ceram. Soc.* **2011**, *94* (8), 2562−2570.
(41) Samsonov, G. V.; Fomenko, V. S.; Kunitskii, Y. A. Thermal Electron Emission from Some Group IV-VI Transition-Metal Borides and Its Relationship to Their Valence-Electron Structure. *Sov. Phys. J.* **1972**, *15* (4), 502−505.
(42) Schulman, D. S.; Arnold, A. J.; Das, S. Contact Engineering for 2D Materials and Devices. *Chem. Soc. Rev.* **2018**, *47* (9), 3037−3058.
(43) Perello, D. J.; Chae, S. H.; Song, S.; Lee, Y. H. High-Performance n-Type Black Phosphorus Transistors with Type Control via Thickness and Contact-Metal Engineering. *Nat. Commun.* **2015**, *6* (1), 7809.
(44) Streetman, B. G.; Banerjee, S. *Solid State Electronic Devices*; Prentice Hall: 2000; Vol. *4*.
(45) Ruppalt, L. B.; Lyding, J. W. Metal-Induced Gap States at a Carbon-Nanotube Intramolecular Heterojunction Observed by Scanning Tunneling Microscopy. *Small* **2007**, *3* (2), 280−284.
(46) Peng, X.; Tang, F.; Copple, A. Engineering the Work Function of Armchair Graphene Nanoribbons Using Strain and Functional Species: A First Principles Study. *J. Phys.: Condens. Matter* **2012**, *24* (7), 075501.
(47) Dutta, S.; Pati, S. K. Novel Properties of Graphene Nanoribbons: A Review. *J. Mater. Chem.* **2010**, *20* (38), 8207−8223.
(48) Choudhury, D.; Mandia, D. J.; Langeslay, R. R.; Yanguas-Gil, A.; Letourneau, S.; Sattelberger, A. P.; Balasubramanium, M.; Mane, A. U.; Delferro, M.; Elam, J. W. Atomic Layer Deposition of HfO2 Films Using Carbon-Free Tetrakis (Tetrahydroborato) Hafnium and Water. *J. Vac. Sci. Technol. A Vacuum, Surfaces, Film.* **2020**, *38* (4), 42407.
(49) Hoekstra, H. R.; Katz, J. J. The Preparation and Properties of the Group IV-B Metal Borohydrides. *J. Am. Chem. Soc.* **1949**, *71* (7), 2488−2492.
(50) Lyding, J. W.; Skala, S.; Hubacek, J. S.; Brockenbrough, R.; Gammie, G. Variable-temperature Scanning Tunneling Microscope. *Rev. Sci. Instrum.* **1988**, *59* (9), 1897−1902.

https://doi.org/10.1021/acsnano.3c02794
ACS Nano 2023, 17, 17771−17778